

# Electronics Adaptation for Scintillation Dosimeter

David Encarnação<sup>1,a</sup>

<sup>1</sup>Faculdade de Ciências da Universidade de Lisboa, Lisboa, Portugal

Project supervisors: Duarte Guerreiro, João Gentil Saraiva, Jorge Sampaio

November 23, 2023

**Abstract.** The paper describes the status of a scintillation dosimeter under development at LIP and FCUL. Correction factors are determined to equalize the response of the different MAPMT hardware channels. A method for translating the MAPMT signals to a quantity in the real world that can be related to dose is studied. In particular, it will evaluate the detector performance using a data acquisition system (TRB3). Measurements using different radiation sources (50 kV X-Ray emitter, Sr-90) are used to gather preliminary data, allowing for their characterization. Before conclusions, a discussion addressing possible future improvements for the scintillation dosimeter is included.

**KEYWORDS:** radiation detector, scintillating fibre array, external clock

## 1 Introduction

### 1.1 The Scintillation Dosimeter

The scintillation dosimeter in study is a detector currently in development at LIP and FCUL. It consists of an array of 64 scintillating plastic optical fibres with a diameter of 1 mm each, juxtaposed side by side in a rectangular panel [1]. Each of these fibres then connects to a different anode of a multianode photomultiplier tube (MAPMT H8500C [2]), so that the radiation that each fibre absorbs can be measured independently. A photomultiplier is a photodetector that increases the current produced by incident photons in  $10^5$  to  $3 \times 10^6$  orders of magnitude. Due to this characteristic some of these photodetectors have a single photon sensitivity, and are normally powered by high voltage power supply ( $> 700$  V) with a negative polarity. The optical fibre array and the MAPMT are housed within a much larger box for safe handling and protecting the fibers and MAPMT from unwanted light exposure that increases background noise during readings [Fig. 1]. This box has a rectangular hole in the front and back, of similar size to that of the array detection region ( $64 \times 100$  mm<sup>2</sup>) for beam entrance. According to the necessity these two passages are closed using a thick plastic slab or thin foils of aluminum. In the current setup a  $< 0.1$  mm thick aluminum wall is used that allows [3] the usage of both a 50 kV X-ray and a Sr-90 radioactive sources in the laboratory experiments being held at FCUL.

### 1.2 Data Taking Options

There are several options, depending on the measurement's purpose, while gathering data with the dosimeter. Laboratory tests have been made with an oscilloscope to analyze pulses in greater detail, with a charge integrator to obtain the total charge of a measurement and with a Time-to-Digital-Converter (TDC) to obtain event counts. In this last case, the data loss regarding the characteristics of each pulse is not considered important, given that the

taken measurements are of the number of events (pulses) in a specified length of time.



**Figure 1.** On the left, the detector as used during the laboratory essays. On the right, the scintillating plastic optical fibre array placed inside it.

### 1.3 Adaptation of the Dosimeter for TRB3 Readout

In order to be able to make measurements using the radiation dosimeter, the MAPMT outputs through SAMTEC connectors (TMM-118-03-G-D), which are coupled to an interface board to extract the signal from each channel through a LEMO00 coaxial cable. Each particle crossing the fibre detector will produce light that is collected by the MAPMT and will result in a small pulse of charge to be sent through the correspondent cable. In the experimental setup at FCUL, each of these cables is connected to a discriminator, which will produce an output signal for each input signal above a user defined threshold, with a user defined width and a fixed amplitude. The discriminator pulses are then sent to a NIM - ECL translator, preparing them to be transferred into the TRB3 [4] platform, the TDC in use [Fig. 2]. The TDC is used to recognize events and register the time at which they occurred, allowing to achieve the previously specified purpose of measuring amount of events per unit of time.

<sup>a</sup>e-mail: davidpires.8@gmail.com

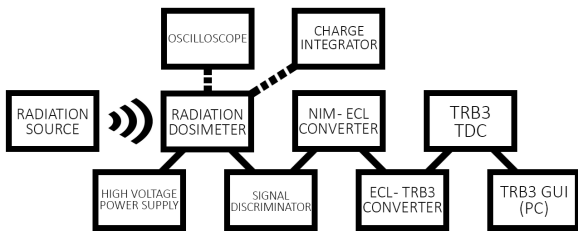


**Figure 2.** Setup diagram with alternative measurement devices connected to the dosimeter by dotted lines.

### 1.4 Measurement-Event Synchronization

The possibility of making external clock adaptation for the TRB3 to allow the platform to automatically synchronize event measurements was considered, but more readily available alternatives were also investigated.

- Discriminator Vetoing - An attempt was made to use the discriminator as a switch to enable and disable the TRB3 using its veto input, however it was unsuccessful.
- TRB3 GUI Modification - In order to take readings using the TRB3, a computer must be connected to a shared router. Then a virtual connection established with the platform and its TDC counting program initiated. The TRB3 then starts hosting a local html site, which after accessed through the computer provides the measured values. The found solution was to implement additional functions into the TRB3's interface, allowing a better control of measuring times and event rate readings.

## 2 Experimental Procedures

Trials in the laboratory are performed using a source of Strontium-90 (Sr-90), which is a radioactive isotope of strontium, or an X-Ray emitter [Fig. 7].



**Figure 3.** On the left, the Sr-90  $\beta^-$  radiation source. On the right, the X-Ray emitter.

### 2.1 Sr-90

The Sr-90 source tends to provide relatively constant amounts of  $\beta$  radiation, due to a long half-life time. This type of radiation consists on the emission of electrons or positrons, more ionising than X-Rays but also less penetrating. Sr-90 experiences  $\beta^-$  decay, meaning it only releases electrons. After decay, the Sr-90 becomes Yttrium-90 (Y-90), which will in turn decay again into stable Zirconium-90 (Zr-90). This transition also releases  $\beta^-$  radiation.

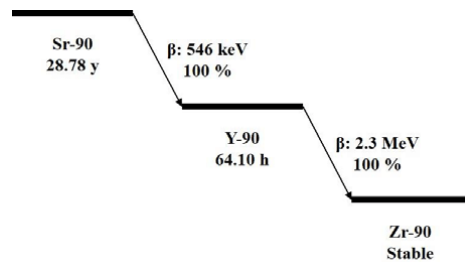


**Figure 4.** Sr-90 decay scheme.

Sr-90  $\beta^-$  emissions have an energy of up to 546 keV [Fig. 4], and up to 2.3 MeV during Y-90 decay. It is, however, a spectrum of emissions, as different electrons may hold different amounts of energy [Fig. 5]. The source of Sr-90 is placed close to the dosimeter, normally around 10 cm away from the case, lined up with the aluminum window.

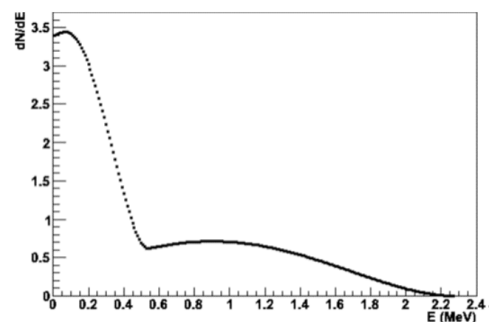


**Figure 5.** Sr-90 emission spectrum.

### 2.2 X-Ray Emitter

Trials using the X-Ray emitter allow for performing measurements with an approximately level exposure across the dosimeter and testing photon radiation detection. The emitter is used in 3-second bursts of radiation emission and has a maximum energy of approximately 50 keV [Fig. 6]. This emitter is fixed and the dosimeter is placed further away from it than when testing with the Sr-90, normally between 35 and 50 cm away.

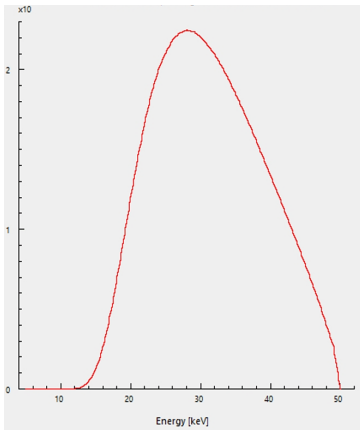


**Figure 6.** X-Ray emitter emission spectrum.

### 2.3 PMMA Phantom

The scintillation dosimeter will be taken to the Netherlands for testing, where it'll be used to measure the amount of protons that collide with the array. In order to allow for more accurate testing, a modification was developed consisting of a PMMA wall [5] to be put between the emitter and the detector with a series of steps to adjust depth (PMMA Phantom). Testing was also conducted with it, however it was not possible to obtain any values with the Sr-90 source, since the PMMA absorbs all  $\beta^-$  radiation before it reaches the fibre array. Experiment data presented in Section 5 was obtained while not using the PMMA Phantom.

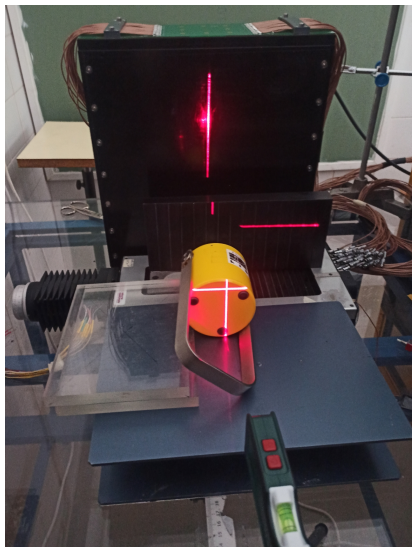


**Figure 7.** Preparing PMMA Phantom test with the Sr-90  $\beta$  radiation source.

## 3 Setup Characterization

The experimental work started by measuring a set of relevant characteristics of the experimental setup. Beginning by measuring the calibration factors needed to equalize the response of all the scintillation dosimeter channels, then making dark current and background noise measurements.

### 3.1 Fibre Grid Energy Calibration Factors

Each individual fibre, due to variations in length, diameter and opacity and naturally occurring surface imperfections, between other unknown factors, has a different capacity to absorb particles which results in different amounts of photons being emitted and therefore detected by the MAPMT, even when exposed to the same type and amount of radiation [6]. Each fiber was tested individually while already in the array, exposing them to X-Ray radiation. A lead plate with a millimeter wide slit was used in order to isolate the targeted fibre and the integral of absorbed energy measured. With these tests, a per-fibre calibration factor was calculated and must be considered in any future measurements [Fig. 8]. To obtain these values, the average of absorbed charge  $\bar{Q}$  was calculated and the factor obtained with  $Q_i/\bar{Q}$ , with  $Q_i$  being the charge absorbed by the fibre in the position  $i$ .

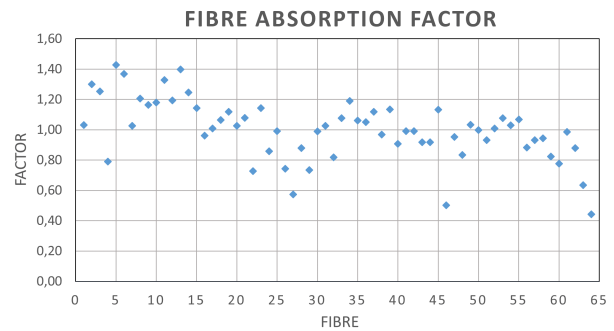


**Figure 8.** Absorption factor per fibre, organized by their positions from left to right on the array.

### 3.2 Dark Current and Other Noise Sources

In order to correct measurements, trials without incident radiation should be made and an average of their results subtracted from the actual experiment's results. These trials should be made under the same high-voltage power source circumstances as the following measurements these adjustments will be applied to. Due to the nature of the electronics that makeup the MAPMT, there's a leakage current that is generated within it when connected to a high-voltage power source. The MAPMT is so sensitive that it detects this current's electrons, causing energy pulses to be sent out that aren't part of the radiation being measured [7], which is called dark current. Other than the noise pulses caused by dark current, there's also background noise which can be induced by the absorption of photons from incident radiation not from the source in study. These are indistinguishable from each other, although the second can be minimized, and precautions were taken during the detector development with this purpose. The noise measurements are presented in Fig. 9.

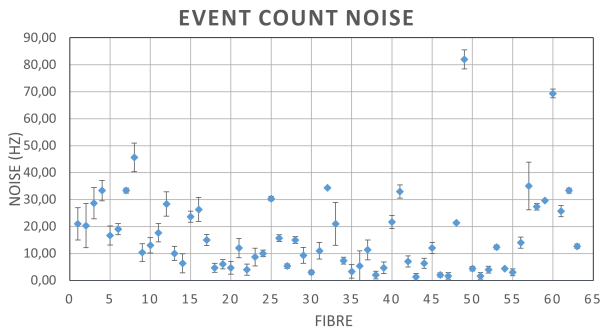


**Figure 9.** Noise per fibre, organized by their position from left to right on the array, in Hz.

### 3.3 TRB3 Frequency Response

Tests have been conducted using a function generator to connect to the TRB3 instead of the MAPMT to verify how accurate its measurements are.

Signal Function Generator Frequency (Hz)	TRB3 Registered Value (Hz)	Relative Deviation
$1 \cdot 10^1$	10.67	6.7%
$1 \cdot 10^2$	106.33	6.3%
$1 \cdot 10^3$	1,069.67	7.0%
$1 \cdot 10^5$	108,112.33	8.1%
$1 \cdot 10^6$	1,072,808	7.3%
$1 \cdot 10^7$	10,650,216	6.5%
$2 \cdot 10^7$	21,640,009	8.2%

**Table 1.** TRB3 test results.

As can be verified from the results presented in Table 1, the TRB3 also seems to have an error associated with its measurements. After performing several tests under the same conditions and obtaining consistent values it should allow for relative comparison between measured values. For a full understanding of this bias more testing will be needed to assess the precision of this data acquisition chain.

## 4 Future Improvements

As the detector is still in its development stage, further improvements have been considered and may be tested in the future. These include:

- Fibre Array Grid - Another fibre array in a perpendicular placement with the current one would make a 2D grid-like detection possible ( $1 \times 1 \text{mm}^2$ ).
- Thinner Fibres - To further improve the spatial resolution of measurements, thinner fibres (0.5 or 0.2 mm) may be used. These may also be square-shaped to provide a flatter detection surface.
- Alternative Photodetector - Other photodetectors with different characteristics may be more appropriate for specific types of measurements.

## 5 Results and Conclusions

### 5.1 Sr-90 Experiments

When exposed to the Sr-90 radiation source, the results show in Fig. 10 were obtained.

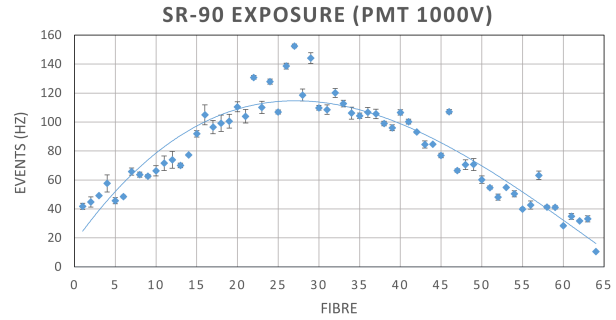


**Figure 10.** Sr-90 exposure results, normalized using the calibration factors after removing noise counts.

The detector measures an average rate of  $(80.31 \pm 2.47)$  Hz, with a maximum of 152.47 Hz and a minimum of 10.55 Hz. A statistical analysis of the measurement data provides a skewness value of 0.067 and a kurtosis value of  $-0.795$ , meaning the graph is lightly skewed to the left and that it has a flatter distribution than a normal distribution, though a peak near the center can still be easily identified. This is expected as the radiation source is smaller than the fiber array’s width. The deviation to the left is likely due to alignment errors during testing.

### 5.2 X-Ray Experiments

When exposed to X-Ray radiation, the results shown in Fig. 11 were obtained.

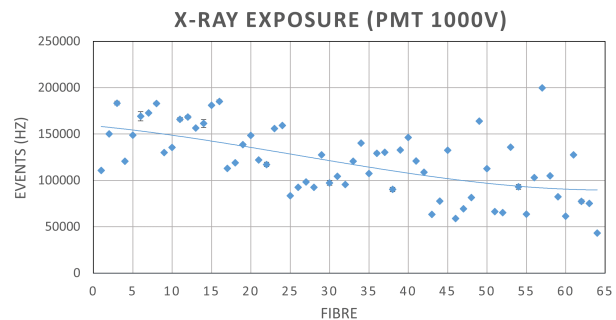


**Figure 11.** X-Ray exposure results, normalized using the calibration factors and field corrections after removing noise counts.

The detector measures an average rate of  $(119,895 \pm 946)$  Hz, a maximum of 199,852 Hz and a minimum of 43,189 Hz. In this case, the skewness value of 0.068 and the kurtosis value of  $-0.783$  are similar to the values obtained with the Sr-90 exposure, however the resulting graph can be observed to be different from the previous, as the radiation field is more linear and decreases from the

left side of the array to the right side. This inclination is not yet fully understood but could be related to some small rotation of the detector. Comparing the obtained event counts with the Sr-90 results, they are several orders of magnitude ( $10^4$ ) higher on average, as expected, since the X-Ray emitter produces much higher photon counts than the Sr-90 source releases electrons. The photons also have the ability to penetrate the aluminum window to a much greater extent.

### 5.3 Conclusions

The dosimeter is close to being finished, requiring merely more fine-tuning and calibration. With a few more tests and possible inclusion of the previously discussed improvements, it can be used for its intended purpose of aiding in biological studies related to the effects of radiation.

### Acknowledgements

A special thanks to the project supervisors and the other members of LIP at FCUL that allowed for this internship

to occur and that are working to aid the development of this project.

### References

- [1] B. Fernandes, *First Measurements with a Scintillating Fiber Microdosimeter* (2022), LIP-STUDENTS-22-08
- [2] *H8500 SERIES / H10966 SERIES Datasheet*, [dtsheet.com](https://www.dtsheet.com)
- [3] G. F. Knoll, *Radiation Detection and Measurement* (2010)
- [4] *TRB3 Documents*, [trb.gsi.de](https://trb.gsi.de)
- [5] D. Salgueiro, *Design of a fiber-phantom detector for quality assurance* (2023), Tese de Mestrado
- [6] M. Borges, *Beam tests of a scintillation array detector for high-resolution dosimetry* (2023), Tese de Mestrado
- [7] International Atomic Energy Agency, *Selected Topics in Nuclear Electronics* (Vienna, 1986)